مجلة جامعة بني وليد للعلوم الإنسانية والتطبيقية

تصدر عن جامعة بني وليد – ليبيا

Website: https://jhas-bwu.com/index.php/bwjhas/index

العدد التاسع والعشرون، 2023

Molecular Docking, DFT, MEPs and in Vitro Investigations of Ni(II), Pd(II) and Cu(II) complexes containing thiosemicarbazone moiety

Amrajaa S. Abubakr [1*], Salima A. BenGuzzi[2], Safaa S. Hassan[3]

[1]Department of Chemistry, University of Ajdabiya, Libya

[2]Department of Chemistry, University of Benghazi, Libya

[3]Department of Chemistry, University of Cairo, Egypt

*Crosspnding author: amrajaa.shahhat@uoa.edu.ly

تاريخ الاستلام: 2023-06-01 تاريخ القبول: 2023-06-18 تاريخ النشر: 2023-09-07

Abstract: Metal complexes of 3-acetylpyridine thiosemicarbazone ligand (3-APT) with Ni(II), Cu(II), and Pd(II) chlorides were screened against bacterial strains *Staphylococcus aureus*, *Bacillus subtilis*, *Escherichia coli* and *Pseudomonas aeruginosa*. Cytotoxic activities showed that the Pd (II) complex exhibited more effective cytotoxic activity against human breast cancer cell line MCF-7 with (IC_{50}=20.72 µg/ml. The nucleophilic and electrophilic location interactions in the investigated ligand were described using the molecular electrostatic potential (MEPs) map. The density functional theory (DFT) was also carried out. Molecular docking investigation displayed the interactions between the active site amino acids of ribosyltransferase with the studied complexes. Besides, the cytotoxic modes of action by the active chelates with epidermal growth factor receptor tyrosine kinase were studied.

Keywords: 3-Acetylpyridine, Thiosemicarbazone, Microbiological screening, Molecular docking.

1- Introduction

Bacterial and viral mutations, as well as resistance to existing drugs, have emerged as significant challenges in the medical field. This necessitates the development of novel drugs and medicines to combat such a threat. It has been observed that metal complexes with thiosemicarbazone (TSC) ligands and their derivatives exhibit respectable medicinal properties and seem advantageous in terms of generating less toxic and more potent medications [1-4]. Significantly, detailed studies have shown that the biological activity of thiosemicarbazones is related to their ability to coordinate with metal centers in proteins and enzymes in a variety of ways, whether in the neutral form of thione or in the negative form of thiol. On chelation, the polarity of the metal ion will be reduced to a greater extent due to the overlap of the ligand orbital and partial sharing of the positive charge of the metal ion with the donor [5]. This increased lipophilicity enhances the penetration of the complexes into lipid membranes and thus blocks the metal binding sites on enzymes of microorganisms [6]. When the nitrogen atom of the imine group of TSCs forms a hydrogen bond with the active centers of cellular components, it may disrupt typical cellular functions. These metal complexes also disturb the respiration process of the cell and thus block the synthesis of proteins, which restricts further growth of the organism [7]. It also correlates with the nature of the N-C=S group, which is of great interest in chemotherapeutics [8]. Palladium has complexes that demonstration a noticeable cytotoxic activity comparable to that of platinum-based drug references [9]. Consequently, the complexes formed by coordination of thiosemicarbazone derivative with various metal ions specially Pd(II) ion are expected

to have potent antitumor properties [10]. However, there are only few previous reports on 3-acetylpyridine thiosemicarbazone [11-14]. So, this work constitutes a fertile and exciting area for further investigations. The present article gives an insight into the antibacterial and antitumor activities of copper(II), nickel(II) and palladium(II) complexes derived from 3-acetylpyridine thiosemicarbazone (3-APT). The nucleophilic and electrophilic location interactions in the investigated ligand were described. The density functional theory (DFT) is also described. The molecular docking study will be completed at the end to demonstrate the various hydrogen bonds that have been formed between our compounds and the selected proteins.

2- Methods

a. Theoretical Method

The investigated complexes are optimized using the density functional theory B3LYP and the basis set LANL2DZ [15]. The structures were visualized using GaussView 5.0.8 after the calculations were completed using the Gaussian09 package [16]. For molecular docking studies, the Molecular Operating Environment (MOE) 2009.10 program was utilized. The binding free energy of the inhibitor inside the macromolecule was calculated. The protein crystal structure of the ribosyltransferase (antimicrobial activity) (PDB: 3GEY) and epidermal growth factor receptor tyrosine kinase EGFR (antitumor activity) (PDB code: 1M17) was obtained from Protein Data Bank (PDB). The nucleophilic and electrophilic location interactions were descripted using the molecular electrostatic potential (MEP) map [17].

b. Experimental Method

In vitro antibacterial activities of the ligand and its complexes were studied using the Kirby-Bauer disc diffusion method [18]. After being incubated at 35–37 °C for 24–48 hours with Gram (+) bacteria like *Staphylococcus aureus* and *Bacillus subtilis* and Gram (-) bacteria like *Escherichia coli* and *Pseudomonas aeruginosa*, the diameters of the inhibition zones were measured in millimeters. The growth of the tested bacteria was reached to approximately 10^7 cells/ml using Mueller Hinton media and counted by using plate counter [19]. The volume used from microbial suspension was 100 µl that spread onto agar plates. The volume used from the tested samples was 10 µl that placed on agar media with the help of blank paper disks. The influence of ligand and their chelates on the used bacteria were compared with sensitivity to a common antibiotic (Gentamicin).

$$\text{Activity Index (A)} = \frac{\text{Inhibition zone of prepared compound(mm)}}{\text{Inhibition zone of standard drug(mm)}} \text{x } 100\%$$

The antitumor activity of 3-APT and its complexes against the MCF-7 breast cancer cell line was established through by MTT assay method which measures the cellular metabolic viability [20]. The MTT assay technique is based on the reduction of the tetrazolium salt MTT to insoluble purple formazan by metabolically active cells, making their activities quantifiable by spectrophotometry. Cells were cultured in 96-well plates and were treated with different concentrations of test compounds after incubation. Another group of cells was treated with small concentrations of doxorubicin, After 48 h treatment, the cells were incubated with MTT (0.5 mg mL^{-1}), and formazan crystals were dissolved in DMSO. Results are expressed in terms of the concentration required to inhibit cell growth by 50% relative to untreated cells (IC_{50}).

3- Results and discussion

a. Theoretical results

In order to better understand how well novel compounds exhibit bioactivity against the target, we can use molecular docking to identify the potential mechanisms of interaction and binding affinities of these therapeutic molecules. We validate the docking procedure by docking the co-crystalized ligand in its binding pocket. The co-crystalized ligand in the ribosyltransferase (code: 3GEY) was P34 (N~2~,N~2~-dimethyl-n~1~-(6-oxo-5,6 dihydrophenanthridin-2-yl)glycinamide. The docking results are seen in (Table 1) and (Figure 1). Side chain acceptor interaction type was observed between the terminal amino group proton with carbonyl oxygen of Thr-A622 amino acid in the case of ligand and with carbonyl oxygen of Asp-A623 in both Cu and Ni chelates. Cu chelate observed various interactions as side chain donor between the N of py ring with terminal amino group of Lys-A518, Backbone acceptor between the terminal NH_2 proton of ligand with Gln-B549 carbonyl oxygen and arene-cation interaction between the aromatic pyridine ring with both (Ly-A518 & His-B550) amino acid residues. Moreover, the aromatic pyridine ring interacts with both His-B550 and the Pd chelate in an arene-cation fashion. Molecular docking study of the standard Gentamicin drug observed high scoring energy value which compatible with its antibacterial activity. It demonstrates the side chain donor interactions of the amino acids Asn-B508 (carbonyl oxygen), Lys-A518 (terminal amino), and Gln-B549 (carbonyl oxygen) with the ring oxygen atoms OH and NH_2It was observed that the OH groups of gentamicin and Gln-B549 (carbonyl oxygen) amino acid had a backbone acceptor interaction type. The redocking results mentioned variable poses with acceptable RMSD values. Most values are lower than 2 Å with high docking score. The best pose with high scoring energy and lower RMSD show interaction between NH group of P34 and Asn-B508 (carbonyl oxygen) as side chain acceptor interaction type manner. The Arene-cation interaction type was observed with His-B550. The previous docking results for Gentamicin and P34 were seen in (Figure 2). The hydrogen bonds values of most of observed results were written in (Table 1). All chelates have more negative scoring energy than the ligand itself. Backbone acceptor was observed in the ligand by hydrogen formation between Gln-767 (carbonyl oxygen) residue with NH proton and Arg-752 with the terminal amino proton. Solvent contact interaction was observed in Cu-L and Pd-L compounds. Ni-L chelate formed the hydrogen bond between the terminal amino protons with Asn-818 residue. Molecular docking study of both cisplatin and doxorubicin against the same protein revealed higher negative scoring energy value for doxorubicin than the cisplatin. The chelates have comparable values to the standard doxorubicin drug. The docking results are seen in (Table 2 and Figure 4). Doxorubicin (OH) interacted with Thr-830 (OH) while the cisplatin (NH_3) was interacted with the main chain oxygen of two different amino acids (Asp-831 and Glu-738). We validate the docking procedure by docking the co-crystalized ligand in its binding pocket. The co-crystalized ligand in the EGFR tyrosine kinase receptor (PDB Code: 1M17 (was 4-anilinoquinazoline (AQ4). The redocking of the (AQ4) revealed good poses with RMSD as seen in (Table 2 and Figures 3, 4). The RMSD is lower than 2 Å with high docking score. The docking results cleared the interaction between the (N1) quinazoline ring of (AQ4) inhibitor with the terminal amino group of Lys-721 amino acid. The hydrogen bond values were mentioned in (Table 2).

DFT calculations were performed for the 3-APT ligand and its complexes. The optimization molecular properties were mentioned in Figures (5, 6) and (Table 3, 4). Some bond lengths were increased as [(N9-C7), (N9-N10) and (C11-S12)] and others were decreased as [(C1-N7), (N10-C11) and (C11-N13)] to optimize the coordination through N9 and S12 donor sites. New bonds were formed due to chelation

as M-N9 and M-S12 bonds in all chelates with the appearance M-Cl bond in palladium and copper chelates. The bond angles of ligand were changed by the coordination to metal ions as pointed out in (Figure 5). Angles surrounding the metal change dramatically when the metal center is changed. The negative charge was mostly delocalized over N7 and S12 atoms with calculated charges -0.176 and -0.07 respectively to form the energetically stable five-membered ring. After coordination, the electron density over the previously mentioned atoms was decreased due to the transfer of charge from the donor sites of ligand to the central metal ions i.e. (L→M). The case of an increase in electron density may be due to the back donations from metal to ligand. These calculated charges converted to [Ni= (-0.217&+0.210), Cu= (-0.221 & +0.092) and Pd= (-0.15 &+0.170)] for N7 and S12 atoms respectively. The metal charges converted to +0.097, +0.067 and -0.083 in the case of Ni, Cu and Pd after coordination respectively. The molecular orbitals are identified as the frontier molecular orbitals (FMOs) as seen in (Figure 6). The HOMO-LUMO energy gap has been identified as an important stability descriptor. The large HOMO-LUMO energy gap is consistent with systems that are stable and have little reactiveness. The orbital frontier eigenvalues and HOMO-LUMO gaps are inserted in (Figure 6). A molecule with a small HOMO-LUMO gap is more reactive and is a softer molecule because the smaller hardness values imply higher reactivity. The complexes were more reactive than the parent ligand, as shown by energy gaps. The negative chemical potential is indicative of their stabilities. The electron cloud of (3-APT)'s HOMO is mainly localized on the aliphatic part concluding the thiosemicarbazone part but LUMO electron cloud extended to both the aliphatic and aromatic parts. The electron cloud with respect to the HOMO orbital was distributed after coordination over the aromatic pyridine ring with the coordination center in case of nickel chelate but distributed over the aliphatic part with the coordination center in case of copper and palladium chelates. The LUMO electron distribution of palladium chelate localized over the whole molecule while in nickel and copper chelates was limited to the aliphatic part with the coordination center. As indicated by the magnitude of their dipole moments, the polarity of the ligand increased after chelation by bonding to palladium (II) metal ion and vice versa by coordination with nickel (II) and copper (II). Many ground state parameters can be calculated using the formulas below:

$I = - E_{HOMO}$ $A = - E_{LUMO}$

Where, I= Ionization potential of the compound, A= Electron affinity of the compound

I (Ionization potential) = $-E_{HOMO}$, A (Electron affinity) = $-E_{LUMO}$

η (hardness)=((I-A))/2,

S (Softness) =1/2η,

μ (Chemical potential) =(-(I +A))/2,

x (absolute electronegativity) =((I + A))/2

Also, we noticed that Ni and Cu chelates had the lowest dipole values (See Table 4). The dipole moment property of a substance classically indicates its polarity. Drug solubility in water increases with increasing the dipole moment, suggesting that dipole moment is a crucial factor in determining drug penetration through the organism's cell membrane and the rate of excretion. The ability of a compound to penetrate the lipid layer of a microorganism more effectively is influenced by its liposolubility, attacking the cell constituents and become more dangerous and toxic in the cellular environment.

The electron density is polarized as seen in the three-dimensional view of MEP. Additionally, we can get the size and geometry of the molecules [21]. MEP is computed to estimate specific structural

reactive sites by the change of color that indicates the electron density along the different positions in the molecule. The red or orange areas indicate locations with high density of electrons while the blue color provides positions with the low electron densities. N7 and S12 atoms have great negative electrostatic potential on the studied ligand, while the rest of the ligand molecule has the highest positive electrostatic potential, as seen in (Figure 7). It means the previously mentioned atoms can attracted to the positive electrostatic potential membrane structure of the cells and are active sites for metal ion coordination. We can say that the investigated chelates exhibit positive electrostatic potential (ESP) maps on their skeletons and negative ESP on its coordination centers, as shown in (Figure 7). Therefore, they can bind tightly into the investigated microorganism having the negatively electrostatic potential. This may be necessary in order to produce an optimal docking pose of the drug inside the binding pocket of the tested microorganism in order to form a stable complex.

b. Experimental results

The organisms used consist of two of each Gram positive (*Bacillus Subtilis*& *Staphylococcus aureus*) and two Gram negative (*Escherichia coli* & *Pseudomonas aeruginosa*). All investigated compounds have at least similar inhibition zone value to the standard antibiotic. The most of inhibition zones exceed the standard antibiotic (*Gentamicin*) against all tested organisms as represented in (Figures 8, 9) and pointed out in (Table 5). Nickel chelate observed the best result against the *Escherichia coli* organism with an inhibition percentage 177.8 % relative to the standard antibiotic values (Gentamicin). The other compounds give 150 %, 155.5 % and 144.4 % for Cu, Pd and ligand respectively that compatible with the docking scores sequence is Ni > Pd ~= Cu > 3-APT. The free ligand was more effective than the standard drug at inhibiting the *Staphylococcus aureus* organism, with an inhibition percentage of 133.3%, but their complexes exhibit weaker antibacterial activity, with respective inhibition percentages of 118.5%, 103.7%, and 100% for Ni, Cu, and Pd complexes. When compared to the values for standard antibiotics, it also saw the best results against the *Pseudomonas aeruginosa* organism with an inhibition percentage of 171.4%. The remaining compounds give 161.9 %, 157.1 % and 157.1 % for Cu, Pd and nickel complexes with the sequence is: 3-APT > Cu > Pd ≈ Ni. Additionally, against the *Bacillus Subtilis* bacterial strain, all chelates and ligand demonstrated appreciable activity, as shown by the values in (Table 6).

The cytotoxicity order is Pd > Cu > L≈Ni depending on the IC_{50} values (See Table 6 and Figure 10). The lower IC_{50} of the compound, the less you consume from this active compound to achieve the favored effect. The most notable cytotoxic activity against the cancer cell was achieved by the palladium chelate. The isoelectronic property of Pd (II) to platinum (II) with similar square-planar geometry as cisplatin, the palladium (II) compounds expected to have a potential to be anti-cancer agent. One of the interesting observation that found, in spite of nickel and palladium are from the same group but palladium indicates more effective inhibition for the progression of cancer cells. It may be due to the facilely process of aquation of the Pd-compounds when enter the cancer cell and consequently inhibit its progress. Also, it may be due to the smaller size of the palladium complex as attached to one molecule of ligand only but nickel metal was attached to two molecules of ligand which maybe affect the membrane permeability of cancer cells and then the cell mortality that is called “cell apoptosis” [22]. The same observation was noticed by comparing nickel and copper activities, both complexes were attached to two ligand molecules but the copper ion with a smaller size than a nickel. Therefore, copper chelate observed a higher cytotoxic effect. The anticancer activity of our compounds was in good agreement with earlier studies that suggested the anticancer effects of sulfur-containing

compounds depend heavily on apoptosis [23]. In a previous study testing the cytotoxic properties of 2-APT ligand, the comparison of the cytotoxic activities indicates that 2-APT shows lower IC_{50} value than 3-APT [24].

Conclusion

The significance of thiosemicarbazones and their metal complexes, apart from their diverse chemical and structural characteristics, stems from not only their potential but also their proved application as biologically active molecules. The antibacterial screening showed the superiority of studied compounds over the well-known standard drug, gentamicin. This could be due to the presence of active function groups as NH_2, NH, and N-pyridine which help in the formation of hydrogen bonds with the active center of cell constituents. In particular, among the three complexes, the palladium (II) complex show noteworthy anticancer activity with a lower IC50 value (IC_{50} = 20.72 µg/ml) than its free ligand.

Abbreviations and Acronyms

TSCs (Thiosemicarbazones), IC_{50} (half-maximal inhibitory concentration), µg/ml (Microgram per milliliter unit), MEPs (molecular electrostatic potentials), L (Ligand) Ni (Nickel), Cu (Copper), Pd (Palladium), MCF-7 (Michigan Cancer Foundation-7), FMOs (frontier molecular orbitals), .

Acknowledgment

The simulation in this work was performed at Cairo University's High-Performance Computing Center (accessed on 30 December 2022).

References

[1] García-Tojal, J., et al., Biological activity of complexes derived from thiophene-2-carbaldehyde thiosemicarbazone. Crystal structure of [Ni ($C_6H_6N_3S_2$) 2]. 2001. 86(2-3): p. 627-633.

[2] Prabhakaran, R., et al., Structural and biological studies of mononuclear palladium (II) complexes containing N-substituted thiosemicarbazones. 2008. 43(2): p. 268-273.

[3] Rodríguez-Argüelles, M.C., et al., Copper complexes of imidazole-2-, pyrrole-2-and indol-3-carbaldehyde thiosemicarbazones: inhibitory activity against fungi and bacteria. 2005. 99(11): p. 2231-2239.

[4] West, D.X., S.B. Padhye, and P.B. Sonawane, Structural and physical correlations in the biological properties of transition metal heterocyclic thiosemicarbazone and S-alkyldithiocarbazate complexes, in Complex Chemistry. 2005, Springer. p. 1-50.

[5] Green, M.A., et al., In vivo quantitative whole-body perfusion imaging using radiolabeled copper (II) bis (thiosemicarbazone) complexes and positron emission tomography (PET). 2022: p. 751-771.

[6] Patil, S.A., et al., Comprehensive Review on Medicinal Applications of Coumarin-Derived Imine–Metal Complexes. 2022. 27(16): p. 5220.

[7] Vashi, K. and H.J.J.o.C. Naik, Synthesis of novel Schiff base and azetidinone derivatives and their antibacterial activity. 2004. 1: p. 272-275.

[8] Pelosi, G.J.T.O.C.J., Thiosemicarbazone metal complexes: from structure to activity. 2010. 3(1).

[9] Matesanz, A.I., I. Leitao, and P.J.J.o.I.B. Souza, Palladium (II) and platinum (II) bis (thiosemicarbazone) complexes of the 2, 6-diacetylpyridine series with high cytotoxic activity in cisplatin resistant A2780cisR tumor cells and reduced toxicity. 2013. 125: p. 26-31.

[10] Milewski, S., H. Chmara, and E.J.A.o.m. Borowski, Antibiotic tetaine—a selective inhibitor of chitin and mannoprotein biosynthesis in Candida albicans. 1986. 145: p. 234-240.

[11] Čobeljić, B., et al., Analysis of the structures of the Cu (I) and Cu (II) complexes with 3-acetylpyridine and thiocyanate. 2014. 69: p. 77-83.

[12] Mendes, I., et al., Structural and spectral studies of thiosemicarbazones derived from 3-and 4-formylpyridine and 3-and 4-acetylpyridine. 2001. 559(1-3): p. 355-360.

[13] Alwi, M.A.M., et al., Gravimetric and electrochemical statistical optimizations for improving copper corrosion resistance in hydrochloric acid using thiosemicarbazone-linked 3-acetylpyridine. 2022. 12(43): p. 27793-27808.

[14] El-Ayaan, U.J.J.o.C.C., Transition metal complexes of 3-acetylpyridine 4 N-(2-pyridyl) thiosemicarbazone (HAPS); structural, spectroscopic, and biological studies. 2012. 65(4): p. 629-642.

[15] Becke, A.D.J.T.J.o.c.p., Density-functional thermochemistry. I. The effect of the exchange-only gradient correction. 1992. 96(3): p. 2155-2160.

[16] Zheng, G., et al., Gaussian 09. 2009: p. 48.

[17] Al-Janabi, A.S., et al., Spectroscopic, anti-bacterial, anti-cancer and molecular docking of Pd (II) and Pt (II) complexes with (E)-4-((dimethylamino) methyl)-2-((4, 5-dimethylthiazol-2-yl) diazenyl) phenol ligand. 2023. 27(3): p. 101619.

]18] Biemer, J.J.J.A.o.C. and L. Science, Antimicrobial susceptibility testing by the Kirby-Bauer disc diffusion method. 1973. 3(2): p. 135-140.

]19] Hassan, S.S.J.A.O.C., Antibacterial, DFT and molecular docking studies of Rh (III) complexes of Coumarinyl-Thiosemicarbazone nuclei based ligands. 2018. 32(3): p. e4170.

[20] Ali, A., et al., Ligand substituent effect on the cytotoxicity activity of two new copper (ii) complexes bearing 8-hydroxyquinoline derivatives: Validated by MTT assay and apoptosis in MCF-7 cancer cell line (human breast cancer). 2021. 11(24): p. 14362-14373.

[21] Abdelaziz, A., et al., Ag (I), In (III), and Sn (II) chelates of azo mesalamine drug: Characterization, DFT studies, molecular docking and biological evaluation. 2023. 37(2): p. e6944.

[22] Salama, S.K., et al., Molecular docking simulation and anticancer assessment on human breast carcinoma cell line using novel bis (1, 4-dihydropyrano [2, 3-c] pyrazole-5-carbonitrile) and bis (1, 4-dihydropyrazolo [4′, 3′: 5, 6] pyrano [2, 3-b] pyridine-6-carbonitrile) derivatives. 2017. 71: p. 19-29.

[23] De Gianni, E. and C. Fimognari, Anticancer mechanism of sulfur-containing compounds, in The Enzymes. 2015, Elsevier. p. 167-192.

[24] Pal, S.J.P., Pyridine: A useful ligand in transition metal complexes. 2018. 57: p. 57-74.

[25] Wang, H., et al., A computational study of adsorption and activation of CO2 and H2 over Fe (1 0 0) surface. 2016. 15: p. 107-114.

Figures and Tables

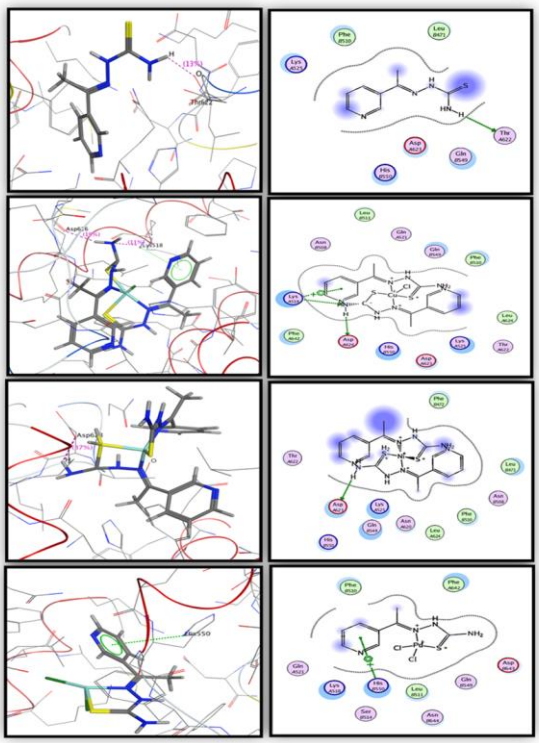

Fig. 1: Docking structures of with proteins

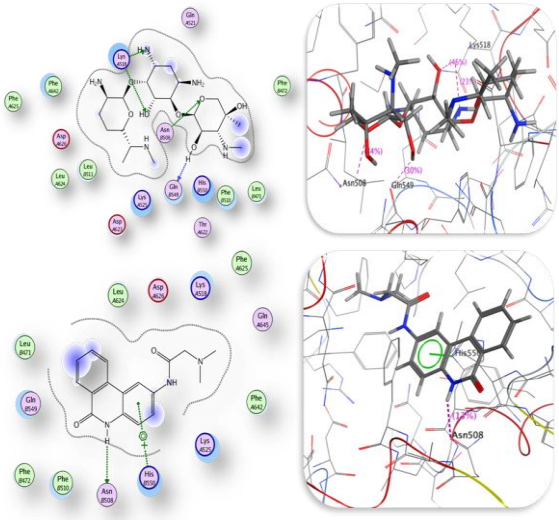

ribosyltransferase.

Fig. 2: 2D and 3D Docking structures of Gentamicin and P34 compounds with ribosyltransferase (code: 3GEY).

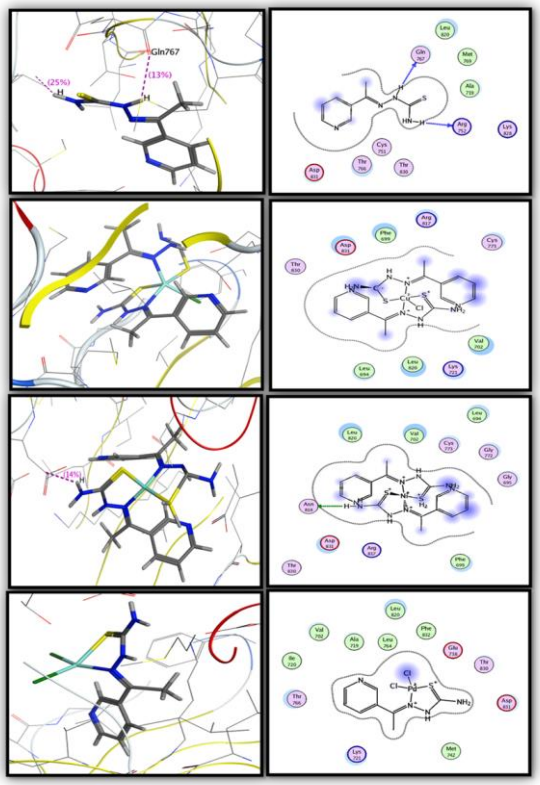

Fig. 3: Docking structures of with proteins EGFR tyrosine kinase.

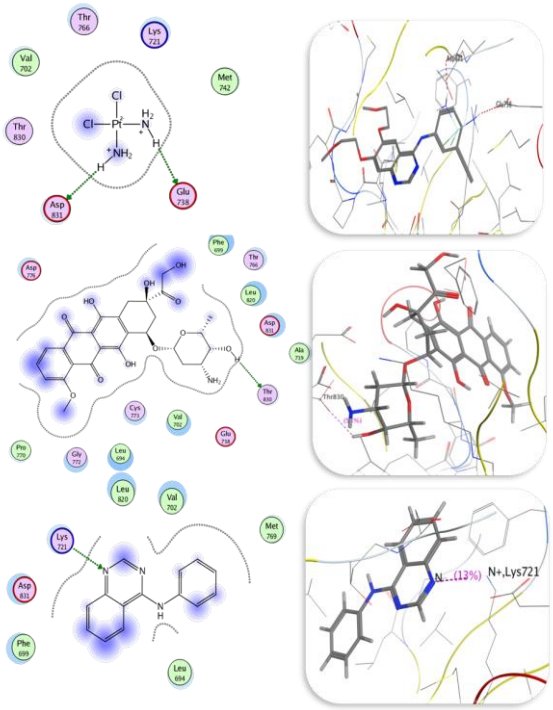

Fig. 4: 2D and 3D Docking structures of cisplatin, doxorubicin and AQ4 compounds respectively against EGFR tyrosine kinase (PDB ID: 1M17).

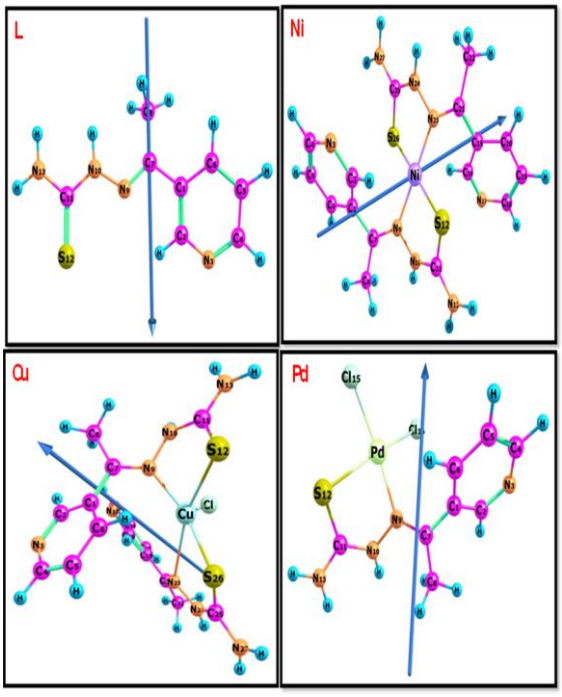

Fig. 5: Optimized geometry of ligand and its metal complexes.

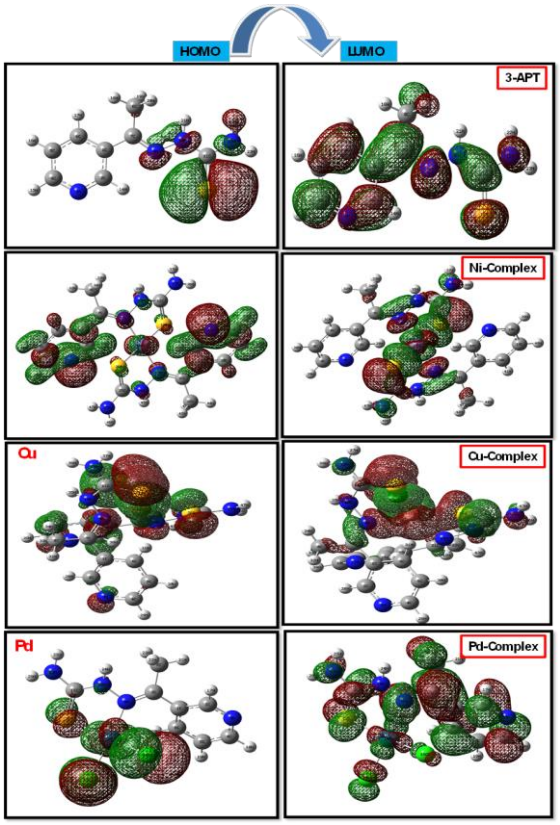

Fig. 6: Molecular graphs of ligand and complexes.

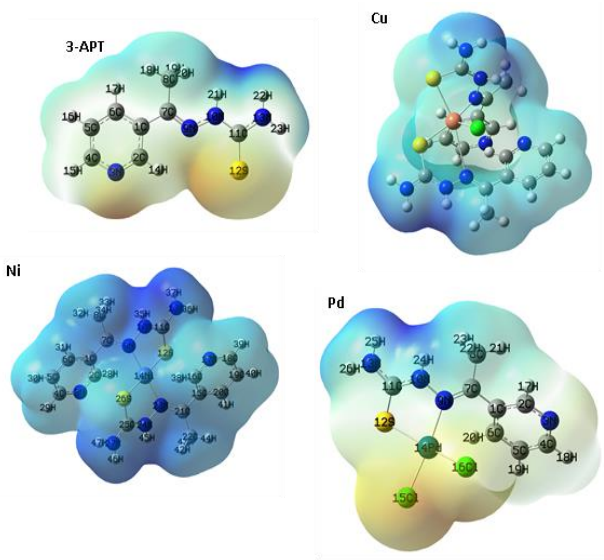

Fig. 7: The molecular electrostatic potentials (MEPs) of the ligand and its metal chelates.

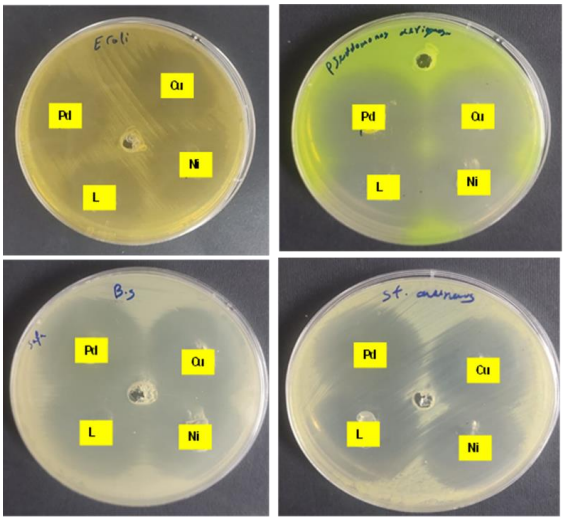

Fig. 8: Photographic representation of zone of inhibition of the ligand and their Ni(II), Pd(II) and Cu(II) towards different types of bacterial strains

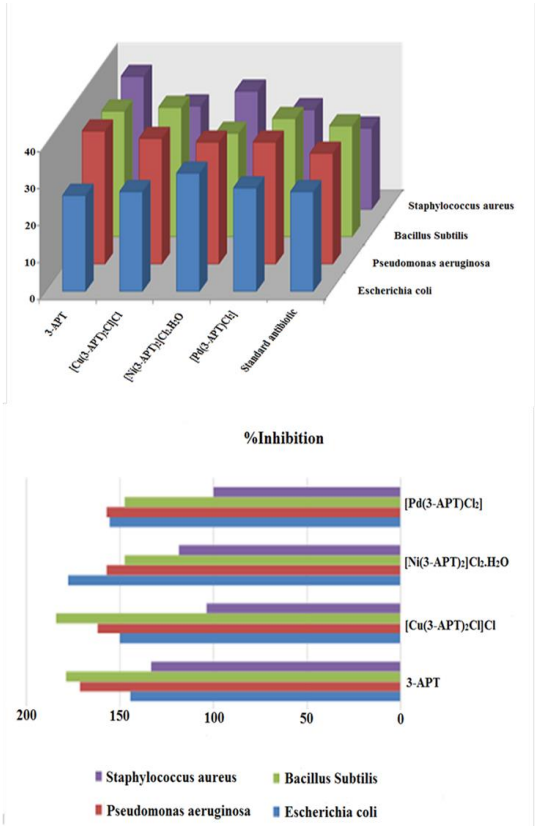

Fig. 9: Biological activity and percentage inhibition of the compounds towards different types of bacterial strains.

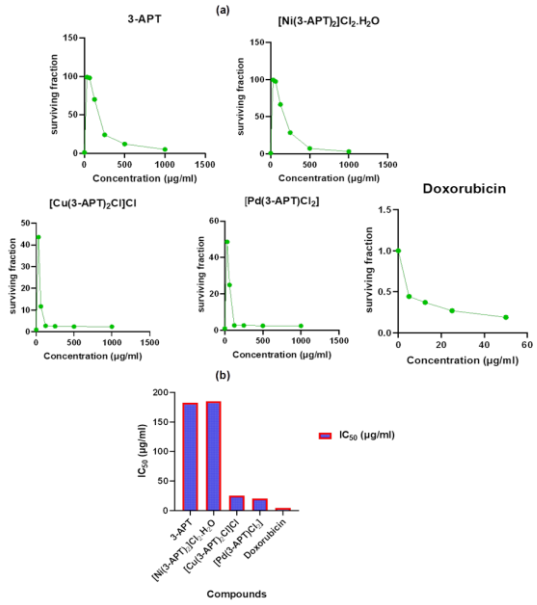

Fig. 10: Surviving fraction of 3-APT ligand and its metal complexes at different concentrations (µg/ml) on MCF-7 human breast cancer cell. B) IC_{50} values against the MCF-7 breast cancer cell line.

Table 1: Comparison of binding affinity of thiosemicarbazone ligand and their complexes against ribosyltransferase.

Compound	Scoring energy (RMSD)	Involved amino acids	Type of interaction
Ligand	-2.60(0.78)	Thr-A622 (2.43 °A)	Side chain acceptor
Cu-Complex	-4.42(2.25)	Asp-A623, Lys-A518 (2.78°A), Gln-B549 (1.88 °A) and (Ly-A518 & His-B550)	side chain acceptor, side chain donor, Backbone acceptor, and Arene-cation interaction
Ni-Complex	-5.71(1.36)	Asp-A623 (1.83 °A)	Side chain acceptor-
Pd-Complex	-2.46(2.53)	His-B550	Arene-cation interaction
Gentamicin	-7.00(1.73)	(Asn-B508 (2.39 °A) & Lys-A518) and Gln-B549 (2.18 °A), Asn-B508 (1.80 °A)	side chain donor and Backbone acceptor, side chain acceptor
P34	-4.78(1.31) -3.31(2.49) -3.25(1.19) -2.66(1.21)	Asn-*B*508 and His-*B*550 N	side chain acceptor and Arene-cation interaction

Table 2: Comparison of binding affinity of complexes against EGFR tyrosine kinase receptor

Compound	Scoring energy (RMSD)	Involved amino acids	Type of interaction
Ligand	-3.04(1.58)	Gln-767 (2.29 °A) and Arg-752	Backbone acceptor
Cu-Complex	-5.57(2.48)		Solvent contact
Ni-Complex	-6.27(1.40)	Asn-818	Side chain acceptor-
Pd-Complex	-4.92(1.03)	His-B550	Solvent contact
Cisplatin	-1.92(2.01)	Asp-831 (2.08 °A) and Glu-738 (1.87 °A)	Side chain acceptor
Doxorubicin	-5.45(2.62)	Thr-830 (2.44 °A)	Side chain acceptor
4-anilinoquinazoline (AQ4)	-3.30(1.26) -3.91(2.54)	Lys-721 (3.30 °A) Lys-721	Side chain donor Arene-cation

Table 3: Some of the optimized bond lengths, Å and bond angles, degrees, for (3-APT) and complexes using B3LYP/6-311G and B3LYP/LANL2DZ respectively.

Bond length (A°)	Ligand	Ni-complex	Cu-complex	Pd-complex
R(M-N9)	-	1.93101	2.01961	2.11753
R(M-S12)	---	2.33752	2.60474	2.46697
R(M-Cl)	---	1.85452	2.32858	2.38765
R(C1-N7)	1.48037	1.46809	1.48031	1.47483
R(N9-C7)	1.30333	1.32968	1.31705	1.32077
R(N9-N10)	1.36739	1.42904	1.42550	1.42078
R(N10-C11)	1.38393	1.36297	1.37943	1.36863
R(C11-S12)	1.71220	1.77562	1.76001	1.75210
R(C11-N13)	1.36616	1.34157	1.35087	1.36231
A(C1-C7-	115.723	119.011	117.53	119.770

N9)			1	
A(C7-N9-Nl0)	119.732	116.951	118.787	116.862
A(N9-N10-Cl1)	121.350	116.416	115.095	119.928
A(N10-Cl1-S12)	125.366	117.854	121.286	122.192
A(N13-C11-S12)	121.728	122.162	121.685	121.124
A(C11-S12-M)	123.293	90.569	83.458	92.015
A(S12-M-N23)		96.833	164.996	---
A(S12-M-N9)	---	83.170	76.729	82.127
A(S12-M-S26)	---	179.994	97.444	---
A(N9-M-N23)	---	179.996	118.269	---
A(S12-Pd-Cl15)	---	55.550	---	91.810
A(N9-S12-Cl)	---	---	95.202	86.695

Table 4: Ground state properties of ligand and its metal complexes using B3LYP/6-311G and B3LYP/LANL2DZ respectively..

Bond length (A°)	Ligand	Ni-complex	Cu-complex	Pd-complex
E_T, Hartree	-927.85681323	-1248.60316966	-1290.70834423	-696.59206139
E_{HOMO}, eV	-5.43	-12.40	-0.33	-5.97
E_{LUMO}, eV	-1.66	-9.11	-0.26	-2.99
ΔE, eV	3.77	3.29	0.07	2.98

I=- E_{HOMO}, eV	5.43	12.40	0.33	5.97
A= - E_{LUMO}, eV	1.66	9.11	0.26	2.99
χ, eV	1.88	6.54	8.16	3.01
η, eV	1.89	1.65	0.04	1.49
S, eV^{-1}	0.27	0.30	13.58	0.34
μ, eV	-3.54	-10.76	-0.30	-4.48

Table 5: Antibacterial activity data in (mm) of ligand and their chelates in various bacteria organisms and comparison with Gentamicin.

Compound	B. subtilis	S. aureus	E.coli	P. aeruginosa
Ligand	34	36	26	36
Cu- Complex	35	28	27	34
Ni-Complex	28	32	32	33-
Pd-Complex	32	27	28	33
Standard antibiotic Gentamicin	19	27	18	21

Table 6: Inhibitory activity (IC_{50}) of the ligand and their chelates against human breast cancer cell (MCF-7).

Compound	IC_{50} (µg/ml)	IC_{50} (µM)
Ligand	182.68	940
Cu- Complex	25.21	48.21
Ni-Complex	185.17	345
Pd-Complex	20.72	55.76